Astron. Astrophys. 354, 67–76 (2000)

ASTRONOMY AND ASTROPHYSICS

The Galactic warp in OB stars from Hipparcos

R. Drimmel, R.L. Smart, and M.G. Lattanzi

Osservatorio Astronomico di Torino, Strada Osservatorio 20, 10025 Pino Torinese, Italy

Received 24 July 1998 / Accepted 16 November 1999

Abstract. The kinematics of distant OB stars perpendicular to the Galactic plane, inferred from proper motions in the Hipparcos catalogue, are analysed and compared to the kinematic signature that would be induced by a long-lived Galactic warp. Previously we reported that the kinematics of the OB stars toward the anticenter were inconsistent with the assumption of a long-lived warp (Smart et al. 1998), showing negative systematic motions as opposed to the expected positive motions. Using a larger sample of OB stars, improved distances, and a more accurate model for the uncertainties, we confirm our previous result for a larger range of galactocentric radii.

However, we note that the new model for errors in the photometric distances reveal an important bias that causes the observed systematic vertical motions to be smaller than their true values. Using synthetic catalogues we investigate the effect of this bias on the systematic vertical motions in conjunction with the possibility of a smaller warp amplitude and a warp precession rate, both of which can also lead to smaller systematic motions. Taken together these three effects can work to produce negative observed systematic vertical motions, similar to those detected in the data, though only with both excessively high precession rates ($-25\,\mathrm{km\,s^{-1}\,kpc^{-1}}$) and very large photometric errors (1 magnitude).

Key words: Galaxy: kinematics and dynamics – Galaxy: structure

1. Introduction

For some time now the existence of a warp in our Galaxy has been well known. First seen in neutral hydrogen emission, it's presence in several other components have since been reported, i.e. IRAS point sources (Djorgovski & Sosin 1989), CO gas (Wouterloot et al. 1990), and dust (Freudenreich et al. 1994). Studies of the Galactic warp have been mostly limited to it's spatial structure (see Binney 1992 for review) because the kinematic signature of a warp primarily manifests itself in the component tangential to the line-of-sight (LOS) of an observer near the Galactic plane, the component that cannot be directly measured by radio observations. For stars, on the other hand, this component is in principle accessible via proper motions, but in practice this approach has been limited by the small magnitude of the expected systematic motion ($\sim$ 1–2 $\mathrm{mas\,yr^{-1}}$), which is smaller than the zonal systematic errors in traditional catalogues. The advent of astrometry from space, inaugurated with the Hipparcos satellite, signals a new era in the study of Galactic kinematics; the high precision ($\leq 1\,\mathrm{mas\,yr^{-1}}$) and accuracy ($< .1\,\mathrm{mas\,yr^{-1}}$) of the proper motions combined with an inertial frame means that it is now possible to detect the kinematic signature expected from a Galactic warp. Once the spatial structure of the warp is determined, its kinematic signature will yield direct information on the precession rate of the warp.

Earlier we reported results from a subsample of the Hipparcos catalogue (Smart et al. 1998). In that study we looked exclusively at distant OB stars toward the anticenter (between 70 and 290 degrees in galactic longitude), expecting such stars to trace the motions of the gaseous component from which they were recently born. Unexpectedly it was found that their kinematics did not follow the predicted signature of a long-lived warp, either precessing or not. This led to the conclusion that either there are additional systematic vertical motions in the Galaxy's gaseous component, or that the warp is not a long-lived structure.

In this contribution we use a larger sample of OB stars from the Hipparcos catalogue to reinvestigate their systematic vertical motions. As before, our interpretation of the data is based upon a comparison between the observed kinematics of the selected sample of OB stars, and the "observed" kinematics of a sample created using a synthetic catalogue generator. The synthetic catalogues are generated based on an assumed statistical model of the (warped) stellar distribution, kinematics and observational errors. By making the identical selections and cuts on the simulated catalogues as are made on the actual data, any biases present or introduced in the sample of OB stars due to errors or selection criterion are likewise reproduced in the synthetic samples as well. In this way the modeled kinematics are translated into observed quantities which can be directly compared with those of the selected sample of stars. In essence, rather than attempting to remove or correct biases in the observed sample, we introduce the same biases into the model in order to determine what is actually detectable.

In the following section the new sample of OB stars is described, while in Sect. 3 the model for the errors used for the

Send offprint requests to: drimmel@to.astro.it

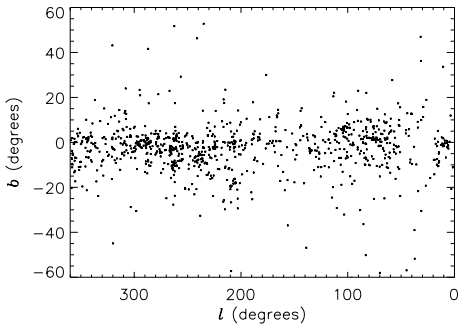

Fig. 1. Distribution of the subsample of 929 distant ($\pi \leq 2\,\mathrm{mas}$) Hipparcos OB stars on the sky with apparent magnitudes brighter than 7.5.

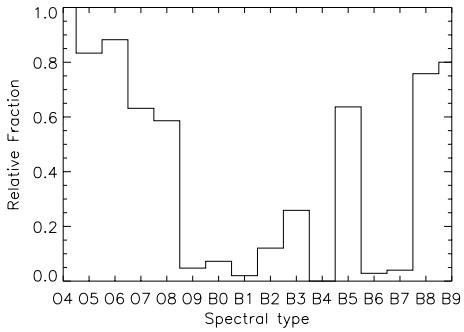

Fig. 2. The distribution of nonLC stars in the north ($\delta > -12.$ deg) with respect to spectral type.

synthetic catalogues is presented. Sect. 4 details an improved estimate of the distances and in Sect. 5, using a simple model for the Galactic warp, we find spatial parameters consistent the distribution of the Hipparcos OB stars. In Sect. 6 we discuss the estimation of the systematic vertical motions, derive the kinematic signature resulting from a long-lived precessing warp, and compare the observed and expected kinematic signatures. Sect. 7 describes the bias introduced in the estimation of the vertical motions by errors in the distance and how these, in conjunction with a smaller amplitude and precession, can produce smaller systematic motions than otherwise expected. We present our conclusions in Sect. 8.

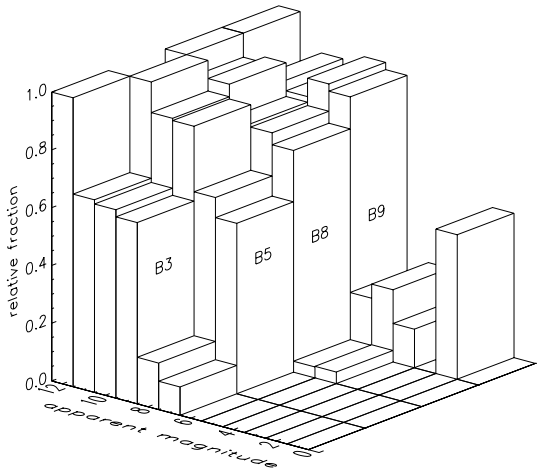

Fig. 3. The distribution of the northern nonLC stars in apparent magnitude for the spectral types B3, B5, B8 and B9.

2. The sample

The sample of OB stars used here to study the Galactic warp is taken from the 10544 OB stars in the Hipparcos catalogue; after excluding 3 stars whose spectral typing is no more specific than "O" or "B", we find 4538 stars with a parallax $\pi \leq 2\,\mathrm{mas}$. Stars with measured parallaxes $\pi < 0$ are retained, as their exclusion would unfavorably bias the sample with respect to distance.

In the Tycho catalogue there are 857 stars brighter than V magnitude 7.5 which do not appear in the Hipparcos catalogue, which has a total of 24384 stars brighter than this magnitude. This suggests that the Hipparcos catalogue is approximately 97 percent complete to this magnitude limit. From our sample alone, based on the distribution of apparent magnitudes brighter than magnitude 7, we estimate that the subsample of 3840 OB stars with $m \leq 7.5$ is 98 percent complete (Smart et al. 1999). Of these brighter stars, 929 have a parallax $\pi \leq 2\,\mathrm{mas}$. Fig. 1 shows the distribution of this subsample of distant OB stars on the sky.

In our earlier work (Smart et al. 1998) purely photometric distances were used. In Sect. 4 we will improve upon these distance estimates, but nevertheless complete spectral classification is needed to calculate a photometric parallax. For the 7279 OB stars with complete spectral classification supplied by Hipparcos, the absolute magnitudes and colors from Schmidt-Kaler (1982) are used to calculate the photometric parallax. For 141 stars without luminosity classification Hβ linewidths were used to determine luminosity class. The 3121 remaining stars without luminosity classification have photometric distances derived from their reddening and estimated absorptions. For further details of these procedures the reader should consult Smart et al. (1997).

In order to understand the properties of the photometric error, the sample of all OB stars brighter than 7.5 will be considered in the following section. These are 3840 in number, with 789 not having an initial luminosity classification (nonLC stars). As we expect that our estimation of the luminosity classes for these stars will be more susceptible to error than those with full spectral classification, it is important to be aware of biases in their distribution. Indeed, because of the use of the Michigan Spectral Survey in the southern sky (Houk & Smith-Moore 1988 and references therein), 745 of the bright nonLC stars (94%) are in the north ($\delta > -12.$ deg). This zonal bias results in a photometric error that is systematically larger in the northern part of the sky than the south, as the following section describes.

To account for the higher photometric error introduced by the nonLC stars, it is necessary to describe their distribution not only on the sky, but also with respect to other relevant variables. Fig. 2 shows the relative fraction of northern nonLC stars with respect to spectral type and Fig. 3 the relative fraction of nonLC stars with respect to apparent magnitude for B9, B8, B5 and

B3 spectral types. The fact that the nonLC stars are primarily restricted to these types, and not hardly seen in types B7, B6, and B4, indicates that the nonLC stars are in general typed at a lower resolution than those stars with luminosity class. For stars of spectral types earlier than B2 the relative fraction of nonLC stars does not vary strongly with apparent magnitude.

While in Sect. 4 only a magnitude cut is applied, in Sects. 5 and 6 two additional cuts are employed; stars with a parallax of $\pi > 2\,\mathrm{mas}$ and a vertical velocity greater than 50 $\mathrm{km\,s^{-1}}$ are removed. The parallax cut is imposed to avoid being biased by local structure, such as Gould's Belt, which dominates the distribution of nearby OB stars. The velocity cut is astrophysically motivated by the presence of runaway stars, which through close encounters have reached escape velocities, and thus do not possess kinematics principally determined by the Galactic potential. The typical threshold detection value for the relative space velocity of runaway stars varies from 40 to 65 $\mathrm{km\,s^{-1}}$ (Blaauw 1993, Torra et al. 1997), thus our value of 50 $\mathrm{km\,s^{-1}}$ applied to one component is conservative, especially as it is approximately seven times greater than the velocity dispersion of this population. The velocity cut is applied to galactocentric radial bins, excluding those stars which deviate from each bin's median velocity by more than $50\,\mathrm{km\,s^{-1}}$, reducing the sample of bright, distant OB stars to 895 in number (less 34), 142 of which are nonLC stars. Meanwhile 255 are cut from all the stars with $\pi \leq 2$, leaving 4283 stars, 1291 of which are nonLC stars. The calculation of the individual and mean vertical velocity is discussed in Sect. 6.

3. Simulated catalogues and improved error model

In order to interpret the observed kinematics of OB stars from the Hipparcos catalogue, a program was developed to generate synthetic catalogues based on a statistical model of the spatial and velocity distributions of the OB stars (Drimmel et al. 1997, 1999). The model distribution is non-axisymmetric, being described by spiral arm segments, most important of which is the local Orion arm, which has a pitch angle of 8 degrees and a spur projecting toward the outer Perseus spiral arm. The synthetic catalogue generator produces catalogues with distributions in galactic longitude and latitude (l, b), apparent magnitude, and proper motion, which closely resemble those of the distant ($\pi \leq 2\,\mathrm{mas}$) OB stars in the Hipparcos catalogue (see also Smart et al. 1997).

The synthetic catalogue generator uses a Galactic dust distribution model based on the 240μm COBE data (Drimmel & Spergel, in preparation) to calculate absorbtions. This model is a refined version of the earlier work of Spergel et al. (1997), adding nonaxisymmetric structure to the dust distribution model, the most important of which is dust associated with the local Orion arm. The added structure in the dust distribution results in additional reddening in the directions tangent to the local arm, thus improving the modeled longitude distributions (see Drimmel et al. 1999 as compared to Drimmel et al. 1997). This same model is used to estimate reddenings and absorptions to the nonLC stars.

Observational errors are modeled for generating observed quantities. The simulated catalogues in Smart et al. (1998) used parallax errors, σ_t, equal to 1 mas, and proper motion errors, σ_μ, were described by simple functions of galactic latitude, as seen in the Hipparcos catalogue (Mignard 1997). These errors are actually better described as varying with ecliptic latitude and apparent magnitude. We have thus improved our model for σ_t and σ_μ by interpolating from Tables 3.2.4-6 given in the first volume of the Hipparcos catalogue (ESA 1997). We have also added a 0.01 magnitude error to the apparent magnitudes. For our purposes here the Hipparcos errors in position (l, b) are negligible.

However, the improvement of the model of photometric distance error makes the greatest difference in the simulated observable kinematics of the synthetic catalogues. Previously our error model involved adding a relative gaussian error of 25 percent of the distance. However, if the errors are normally distributed in absolute magnitude, it is the errors in the distance modulus that are normally distributed. We now model the error in photometric distance by assuming a normal distribution of errors in the absolute magnitude. This error is not only the result of the intrinsic scatter of absolute magnitudes, termed "cosmic error", but also due to errors introduced by uncertainties in the determination of the absorption, intrinsic scatter in the colors, and misclassification errors. Not all these errors are guaranteed to be gaussian.

The photometric error of our observed sample of stars is evaluated using the photometric parallax π_P verses trigonometric parallax π_t distribution for the sample of 3840 OB stars brighter than 7.5. Fig. 4 shows the π_P–π_t distributions for the north and the south. The degraded photometric parallaxes of the north, due to the presence nonLC stars, are responsible for the larger scatter as compared to the south. To illustrate this effect Fig. 5 shows the π_P–π_t diagrams for the north decomposed into the stars with and without luminosity class. It can be seen that the northern stars which possess full initial classification (Fig. 5 left) have approximately the same scatter as the southern stars (Fig. 4 right), and we will assume the same error model can be used for both. One difference between the northern and southern stars with full initial classification is a systematic bias of π_P in the south for stars with π_t centered at 7.5 mas. This bias is due to the presence of stars in the direction of ρ Ophiuchus whose absorptions are systematically overestimated.

Assuming that the observational errors in the Hipparcos trigonometric parallax are well described, we can estimate the photometric error using the synthetic catalogue generator, comparing observed and generated π_P–π_t distributions. For the northern stars with luminosity classification an error model which approximately reproduces the observed distribution of trigonometric and photometric parallaxes is

$$\sigma_M = .5 + \max(0, (m - 6.5)/6) - M/12, \qquad (1)$$

where the apparent magnitude term can be interpreted as being the result of a higher occurrence of classification error at fainter magnitudes, and the absolute magnitude term can be interpreted as an increasing cosmic error and/or uncertainty for the more

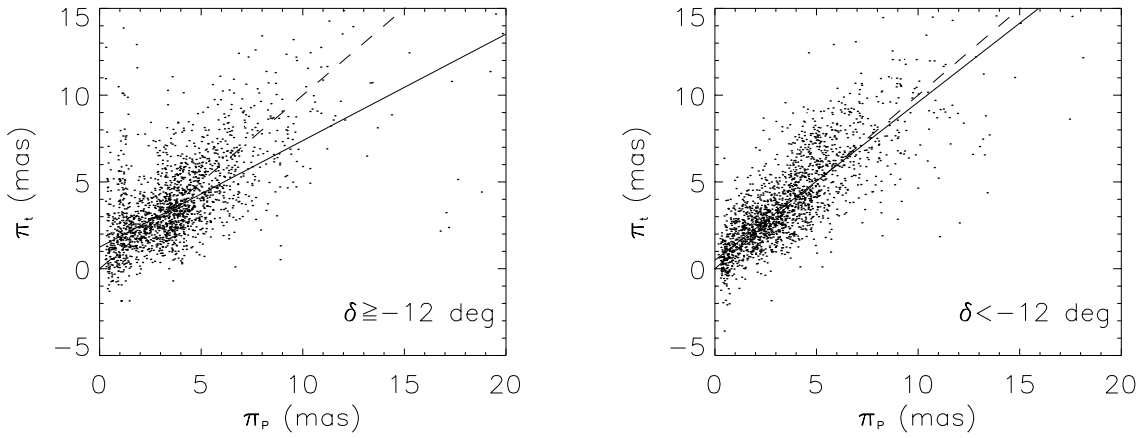

Fig. 4. Photometric versus trigonometric parallax distributions of the bright ($m < 7.5$) Hipparcos OB stars for the north ($\delta > -12.$ deg) and south. The dashed line has a slope of 1, given as reference, while the solid line is the result of a robust linear fit that minimizes the absolute deviations (no points excluded).

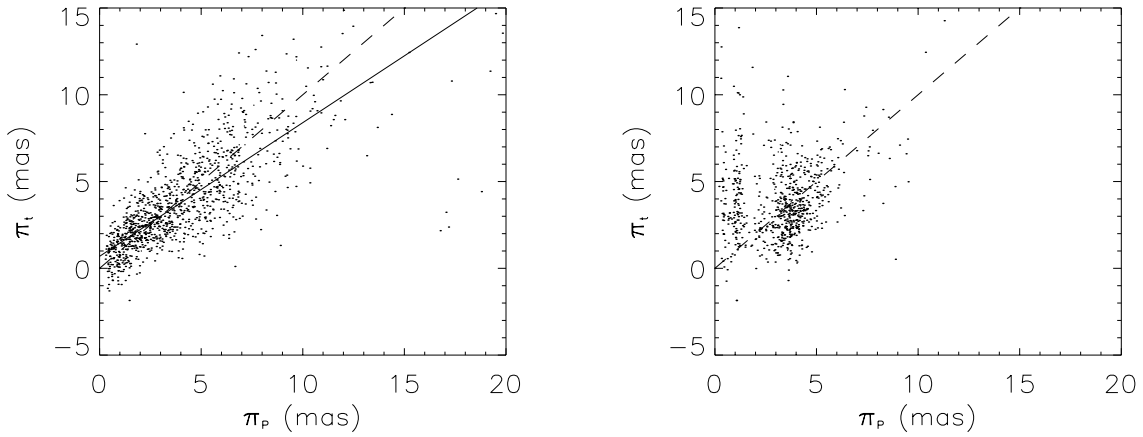

Fig. 5. The photometric-trigonometric parallax distributions of the bright Hipparcos OB stars in the north, decomposed into stars with initial luminosity classes (left plot) and without initial luminosity classes (right plot). Dashed and solid lines are as in the previous figure.

luminous stars. To characterize the distribution a robust linear fit is made to the observed $\pi_{\rm P}$–$\pi_{\rm t}$ distribution in the north (Fig. 5), giving a slope of 0.77 and a mean absolute deviation in $\pi_{\rm t}$ of 1.28, after 17 stars are excluded whose absolute deviations in $\pi_{\rm t}$ are greater than 6 mean absolute deviations (presumably misclassified stars). Meanwhile the modeled distribution (Fig. 6) produces a slope of 0.80, with 1.06 being the mean absolute deviation. For comparison, Fig. 7 shows the $\pi_{\rm P}$–$\pi_{\rm t}$ distribution for a model generated with a purely gaussian magnitude error of $\sigma_M = 1$ magnitude, showing that such a high error does not reproduce well the observed $\pi_{\rm P}$–$\pi_{\rm t}$ distribution.

For the nonLC stars the signatures due to misclassification are prominent, its nongaussian nature leaving clear artifacts in the distribution, especially at $\pi_{\rm t} > 2\,{\rm mas}$ and $\pi_{\rm P} < 3\,{\rm mas}$ (Fig. 5 right). These are intrinsically dim stars incorrectly assigned a high luminosity. In contrast, intrinsically bright stars misclassified as low luminosity stars do not produce clear signatures, but do cause stars of low $\pi_{\rm t}$ to be systematically biased toward higher $\pi_{\rm P}$. We model the misclassification errors as offsets to the true absolute magnitudes, with a binned gaussian probability of misclassification.

However, before applying such errors the distribution of nonLC stars must be modeled. The synthetic catalogue generator does not at this time generate colors, so spectral types were simply correlated with the main sequence absolute magnitudes to infer a model of the distribution of nonLC stars in the north. Fig. 8 shows the model of the relative fraction of nonLC stars in the north. Once a star is randomly determined to be nonLC, a binning error is calculated using

$$p = {\rm int}(1.5N + 3{\rm log}d_0 + 1.4), \qquad (2)$$

where N is a gaussian deviate of unit variance and d_0 the true distance, $(3{\rm log}d_0 + 1.4)$ being a bias reflecting that nearby stars are more likely to be given an over-luminous classification, and distant stars a under-luminous classification. The resulting index p is then used to indicate the appropriate offset, as given in Table 1. In addition to this offset, gaussian noise of $\sigma_M = 0.3$ magnitude is added to the absolute magnitudes.

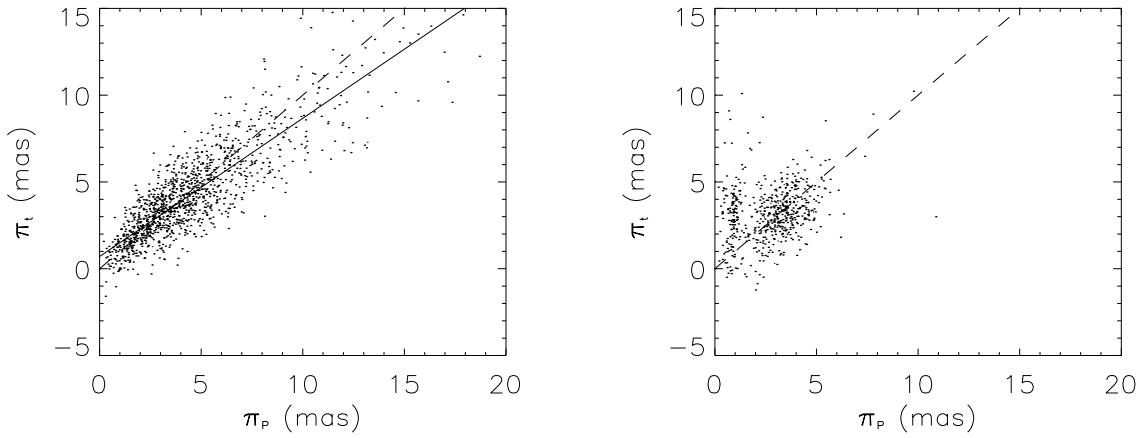

Fig. 6. Modeled photometric-trigonometric parallax distribution of bright OB stars in the north, for LC and nonLC stars (left and right plots respectively), as produced by the synthetic catalogue generator. Dashed and solid lines are as in the previous figures.

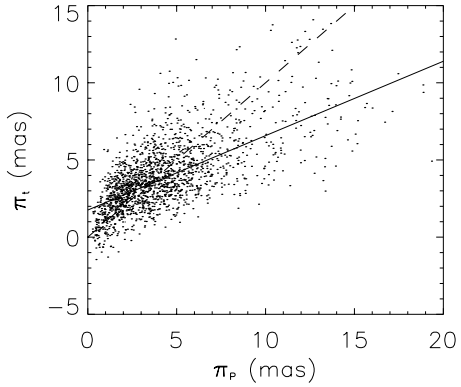

Fig. 7. Modeled photometric-trigonometric distribution of bright OB stars in the north assuming $\sigma_M = 1$ magnitude. Dashed and solid lines are as in previous figures.

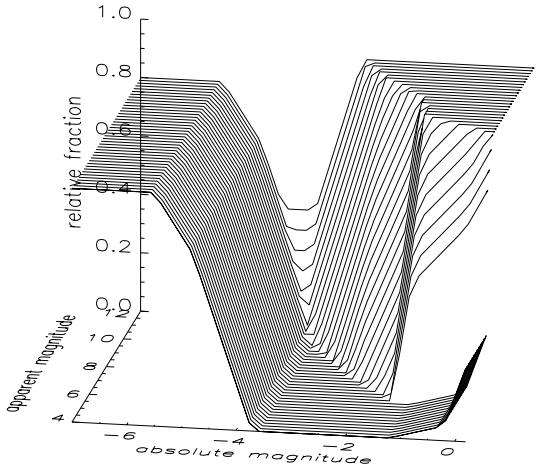

Fig. 8. Model of the relative fraction of nonLC stars in the northern part of the sky, as used in the synthetic catalogue generator.

Much of the added complexity of misclassification in the nonLC stars will not be needed in what follows, as for stars with $\pi \leq 2\,\mathrm{mas}$ only the positive offsets will contribute significantly to the error.

4. Improved distances

In order to improve upon the distances, a distance estimate is used that corresponds to the weighted mean parallax of the trigonometric and photometric parallaxes:

$$\frac{1}{d} = \pi_\mathrm{w} = \frac{\pi_\mathrm{t}/\sigma_\mathrm{t}^2 + \pi_\mathrm{P}/\sigma_\mathrm{P}^2}{1/\sigma_\mathrm{t}^2 + 1/\sigma_\mathrm{P}^2}, \tag{3}$$

where $\sigma_\mathrm{P} = \pi_\mathrm{P}\sigma_M/2.17$ (Smith 1985), and σ_t is interpolated from Tables 3.2.4-6 in volume one of the Hipparcos catalogue. For this distance estimate stars with initial full spectral classification are assumed to have a σ_M as specified by Eq. (1), while nonLC stars are assigned $\sigma_M = 3$ magnitudes. This prescription is used for both synthetic and observed catalogues.

To test whether this new distance estimator is more or less biased than the photometric distance alone, the synthetic catalogue generated in the previous section for the northern sky is used to compare the estimated distance with the true distance. Figs. 9 and 10 show the result of this Monte Carlo test; for stars with an initial luminosity class, the variance and skew of the deviations from a robust linear fit to the photometric distances, are 2.02 and 1.04, while with the new distance estimate they are

Table 1. Modeled offsets in absolute magnitude due to misclassifications, used according to value of the binning error parameter p generated according to Eq. (2).

p	offset	Magnitude range	Misclass.
-4	$-6.8 - M$		V $\rightarrow$ Ia
-3	$-5 - 2M/2.45$		V $\rightarrow$ Ib
-2	-1	$M > -1.2$	V $\rightarrow$ III
	$-(5.9 + M)/2.45$	$M \leq -1.2$	III $\rightarrow$ II
-1	$-3 - M/2.45$		V $\rightarrow$ II
1	1.		III $\rightarrow$ V
>1	1.	$M > -3.1$	III $\rightarrow$ V
	2.5	$-5.2 < M \leq -3.1$	II $\rightarrow$ V
	3.5	$M \leq -5.2$	I $\rightarrow$ V

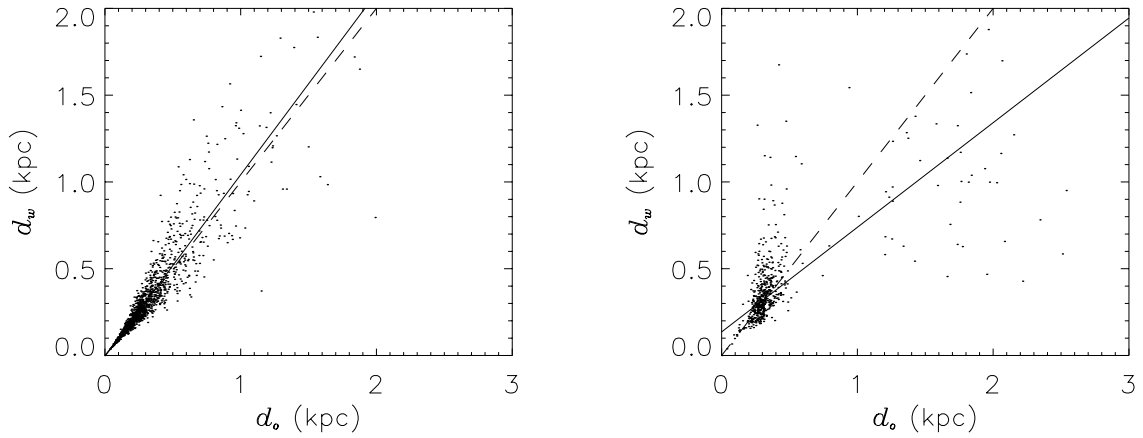

Fig. 9. True versus weighted mean distance (Eq. (3)) of stars in a synthetic catalogue for stars with initial luminosity class (left plot) and nonLC stars (right plot). Dashed and solid lines are as in previous plots.

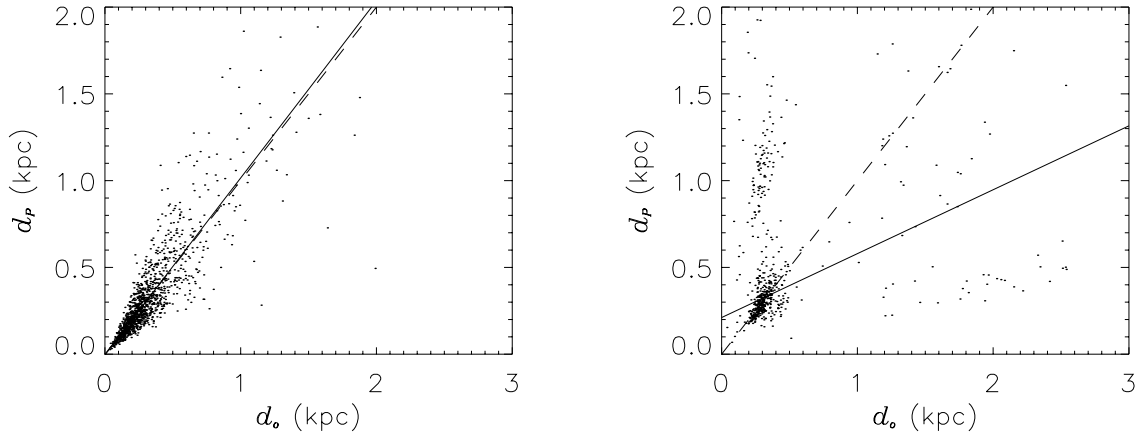

Fig. 10. True versus photometric distance of stars in a synthetic catalogue for stars with initial luminosity class (left plot), and nonLC stars (right plot) where misclassification artifacts are evident. Dashed and solid lines are as in previous plots.

0.41 and -0.07 respectively, showing that the uncertainties are effectively reduced. The slopes and intercepts of both distance estimates show no significant systematic biases. For the nonLC stars the new distance estimator reduces the scatter produced by misclassifications, though their distances can still have significant error.

Using the typical errors $\sigma_M = .7$ and $\sigma_\mathrm{t} = 1.2\,\mathrm{mas}$, the error of π_w for a star at $\pi_\mathrm{t} = \pi_\mathrm{P} = 1\,\mathrm{mas}$ is about 0.3 mas, for which the distance estimate would be $1^{+.45}_{-.24}\,\mathrm{kpc}$. We also point out that for stars in our $\pi_\mathrm{t} \leq 2\,\mathrm{mas}$ sample, the photometric distance will dominate in Eq. (10), as it is only at a distance of $d = \sigma_M/(2.17\sigma_\mathrm{t})$ that $\sigma_\mathrm{P} = \sigma_\mathrm{t}$.

5. Warped spatial distribution

As the Sun is near the line of nodes of the Galactic warp the vertical deviation from the Galactic plane is small, but a local slope with respect to the Galactic plane is produced in the stellar distribution. Using the subsample of the 894 bright ($m \leq 7.5$ magnitudes), distant ($\pi_\mathrm{t} < 2\,\mathrm{mas}$) OB stars, the slopes of the stellar distribution are found in the heliocentric coordinates z and y, y being taken in the direction of rotation, for bins in galactocentric radius r, ($r_\odot \equiv 8\,\mathrm{kpc}$). The slopes were found using a standard robust linear fitting routine which minimizes the absolute deviations in y. In Table 2 we express these slopes as a tilt angle θ, corresponding to the tilt of a galactocentric ring whose axis of tilt goes through the Sun, consistent with the assumption that the line of nodes of the Galactic warp goes through the Sun.

It is well known that OB stars are preferentially found in associations, resulting in a "clumpiness" of the distribution on a larger scale than would be found in a kinematically relaxed population. Nevertheless, we do not expect the presence of associations to affect our results above, as we are describing the overall distribution of OB stars on a scale significantly larger than the size of a typical association. To test this presumption stars which were found to be within the spatial limits of a given association were identified. For this purpose the positions (l, b, d) and limits $(\pm\Delta l, \pm\Delta b)$ for 38 associations were taken from the summary list in Lang (1992), while the line-of-sight extent of each association ($\Delta d = d\max(\Delta l, \Delta b)$) was doubled to take into account possible errors in the distance. Only four associations have ten or more stars from our complete subsample, these being the

Table 2. Angular tilts, θ, of galactocentric rings, in units of degrees, implied by the distribution of bright ($m \leq 7.5$), distant Hipparcos OB stars in heliocentric z and y coordinates. ($\theta = \arctan b$, where $z = a + by$) For the warped and non-warped cases (Columns 4, 5, and 6) the tilts and uncertainties are the means and standard deviations of 30 simulated catalogues. The warped cases (Columns 5 and 6) were generated with $r_{\rm w} = 6.5\,{\rm kpc}$ and $r_{\rm h} = 15$ and 30 kpc respectively (see Eq. (4)). Column 2 gives the number of stars in each bin for the data; the 92 stars not appearing in the table are outside the range of the bins.

Bin (kpc)	N	Data	No warp	Warp	$1/2$ Warp
$6.5< r <7.5$	140	-0.39	-0.24 ± 0.94	0.34 ± 0.91	0.29 ± 0.73
$7.5< r <8.5$	500	1.67	-0.34 ± 0.44	1.08 ± 0.49	0.25 ± 0.44
$8.5< r <9.5$	161	2.05	0.07 ± 0.93	2.54 ± 0.86	1.45 ± 0.80

Cygnus 7 (10 stars), Carina (13 stars), Cepheus 2 (19 stars), and Orion (17 stars) associations, where a total of 102 stars are found inside all associations. Removing each of these sets of stars in turn, the tilts were redetermined. It was found that only one of the associations (Cepheus 2) influenced the measured slopes by more than 0.5 deg.

A warp is effected in the modeled distribution by describing the vertical distribution as a function of $z' = z - Z_{\rm w}(r,\phi)$, where the function $Z_{\rm w}(r,\phi)$ describes the spatial form of the warp in galactocentric cylindrical coordinates, ϕ being taken in the direction of rotation. From radio observations the warp is seen to be symmetric out to about $r = 16\,{\rm kpc}$, and can generally be described by

$$Z_{\rm w} = h(r)\sin(\phi - \phi_{\rm w} + \omega_{\rm p} t), \tag{4}$$

$\phi_{\rm w}$ being the phase of the warp, and $\omega_{\rm p}$ the precession rate of the warp in the direction *opposite* to Galactic rotation, and with

$$h(r) = \begin{cases} (r - r_{\rm w})^2/r_{\rm h}, & r > r_{\rm w} \\ 0, & r \leq r_{\rm w} \end{cases} \tag{5}$$

being a height function parameterized by $r_{\rm h}$ and the radius at which the warp starts, $r_{\rm w}$. The radio observations show that the Sun lies close to the line of nodes, that is, $|\phi_{\rm w}| < 10$ degrees. As the systematic velocity is not sensitive to $\phi_{\rm w}$ in this range (Smart & Lattanzi 1996) we have assumed $\phi_{\rm w} = 0$ in this study. The assumption of a long-lived warp is effectively implemented by taking $\omega_{\rm p}$ to be a constant with respect to r and time t.

Table 2 shows the mean tilts obtained from thirty synthetic catalogues with and without a warp, one warped distribution being generated with the parameters $r_{\rm h} = 15\,{\rm kpc}$ and $r_{\rm w} = 6.5\,{\rm kpc}$, while a second model with half this amplitude ($r_{\rm h} = 30\,{\rm kpc}$) is also shown for comparison. The first set of parameters produce tilts that are consistent with the observed tilts, and these are adopted as our estimated warp parameters in what follows. As noted in our earlier work, the observed tilts indicate a Galactic warp starting within the Solar Circle.

The use of a robust linear fitting routine does not provide formal errors on individual fits, hence no error is given on the tilts of the data. In the case of the synthetic catalogues we have the freedom to directly evaluate the uncertainty by generating multiple catalogues, as we have done. Inasmuch as the synthetic catalogues are accurate statistical representations of the observed data, the uncertainties of their tilts will be representative of the uncertainties in the tilts of the observed catalogue. However, the synthetic catalogues do not include the clumpiness due to the presence of OB associations, which will increase the uncertainties. The 0.5 deg influence of the Cepheus 2 association on the tilts can be taken as an estimate of the probable additional random error that should be added to the uncertainties quoted in Table 2. In any case, the observed tilts are significant and inconsistent with the no-warp hypothesis.

Having estimated the parameters that describe the spatial form of the warp in the OB stars, we are now prepared to consider the kinematic signature accompanying such a warp.

6. Kinematic signature of the warp

The presence of a long-lived warp in the stellar disk will result in systematic motions perpendicular to the Galactic plane; for an observer in the plane of the Galaxy such motions will be primarily observable in the galactic latitude component of the proper motion. Taking $\mathbf{x} = (\cos l\cos b, \sin l\cos b, \sin b)$ as the unit pointing vector to a star, the unit vector tangential to the line-of-sight (LOS) in the direction of increasing galactic latitude is

$$\mathbf{b} = \frac{\mathbf{x}\times(\mathbf{k}\times\mathbf{x})}{|\mathbf{x}\times(\mathbf{k}\times\mathbf{x})|} = \frac{\mathbf{k} - \mathbf{x}\sin b}{\cos b}, \tag{6}$$

where $\mathbf{k} = (0,0,1)$, the unit vector perpendicular to the Galactic plane. The component of a star's relative motion in the direction of $\mathbf{b}$ is

$$(\mathbf{v} - \mathbf{v}_\odot)\cdot\mathbf{b} = 4.74 d\mu_b, \tag{7}$$

where $\mathbf{v}_\odot$ is the solar motion, $\mathbf{v}$ the star's velocity with respect to the local standard of rest (LSR), d and μ_b being the distance in kiloparsecs and the galactic latitude proper motion in $\mathrm{mas\,yr^{-1}}$ respectively. Taking $\mathbf{v}_\odot = (U,V,W)_\odot$ and $\mathbf{v} = (U,V,W)$, defined in the same right hand coordinate system as $\mathbf{x}$, one can write from Eqs. (6) and (7):

$$W = \frac{4.74 d\mu_b}{\cos b} + W_\odot + (S - S_\odot)\tan b, \tag{8}$$

where S is the component of the star's velocity parallel to the Galactic plane and in the plane that contains the LOS and is at right angles to the Galactic plane, that is $S = U\cos l + V\sin l$, and similarly for $S_\odot$. Since distant stars are being considered,

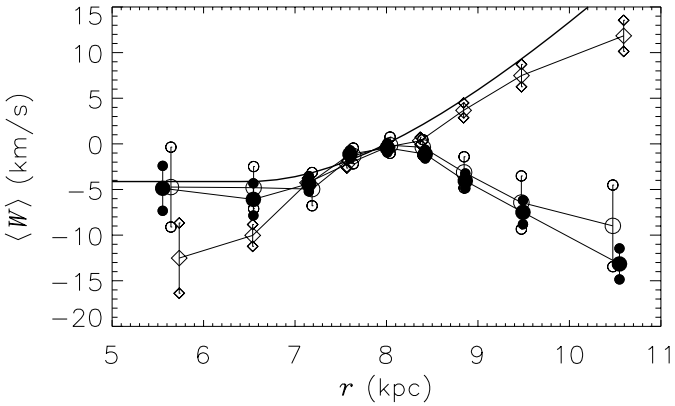

Fig. 11. The systematic vertical velocity $\langle W \rangle$, relative to the LSR, with respect to galactocentric radius. Filled circles are for 4250 distant Hipparcos OB stars to 13th magnitude, while open circles show the signal from the complete portion of our sample (894 stars to magnitude 7.5). The thick solid line is $\overline{v}_z(r) - \overline{v}_z(r_\odot)$ (using Eq. (11)), the velocity along the line of nodes for a long-lived non-precessing warp with an amplitude consistent with the observed spatial distribution, while the diamonds show the observable signature from a single simulated catalogue with the same warp parameters. The symbols show the median W in each radial bin, and their error bars are the standard deviation of the mean of W. The size of the bins increase exponentially from $r_\odot = 8\,\mathrm{kpc}$ with a incremental factor of $\mathrm{e}^{\cdot 2}$, with the exception of the first and last bins that are $\mathrm{e}^{\cdot 6}$ larger.

we do not wish to assume that the stars are in the solar neighborhood (Oort's approximation), and S will therefore contain a contribution from both differential Galactic rotation and the star's peculiar motion. Neglecting the peculiar velocity contribution for the moment, we can write

$$S = \left(\overline{v}_\phi \frac{r_\odot}{r} - v_{\mathrm{LSR}}\right) \sin l, \tag{9}$$

where $\overline{v}_\phi$ is the average rotational velocity of the stellar population, and $v_{\mathrm{LSR}} = 220\,\mathrm{km\,s^{-1}}$. Because the OB stars do not follow Stromberg's asymmetric drift equation (Dehnen & Binney 1998), we simply take $\overline{v}_\phi = v_{\mathrm{LSR}} - 3.0(r - r_\odot)$, found to be consistent for this stellar population (Drimmel et al. 1997).

Finally, adopting $(U, V, W)_\odot = (9, 5, 7)\,\mathrm{km\,s^{-1}}$ (Drimmel et al. 1997), with positive U being radially inwards, we can calculate an observed W for each star using Eq. (8). (Our adopted value for the Solar Motion is comparable with other recent determinations (i.e. Dehnen & Binney 1998), but it should be noted from Eq. (8) that $W_\odot$ enters only as an offset term.) The stars are binned in galactocentric radius to find the observed systematic vertical velocity $\langle W \rangle$ as a function of r; this is shown in Fig. 11. The agreement of the complete portion of our sample with the entire sample is consistent with the assumption that stars fainter than 7.5 form a kinematically unbiased sample.

By ignoring the peculiar stellar velocities parallel to the Galactic plane, S_*, in Eq. (9), we have effectively ignored a $\langle S_* \tan b \rangle$ contribution in each bin. This is done from necessity; we cannot calculate S_* for stars from the Hipparcos catalogue as we do not have their complete space motion. However, from Monte Carlo tests we find that $\langle S_* \tan b \rangle$ is typically less than $0.05\,\mathrm{km\,s^{-1}}$.

We now compare the observed vertical systematic velocities $\langle W \rangle$ with those expected from a long-lived warp. As the vertical velocity W of each star is with respect to the LSR, $W = W_* + \overline{v}_z(r, \phi) - \overline{v}_z(r_\odot, 0)$, W_* being the star's peculiar vertical motion, and $\overline{v}_z(r, \phi)$ the systematic vertical velocity at (r, ϕ) resulting from the warp. Upon averaging $\langle W \rangle = \overline{v}_z(r, \phi) - \overline{v}_z(r_\odot, 0)$, the difference in the systematic vertical motion at the star's and the Sun's position.

To find the systematic vertical velocity $\overline{v}_z(r, \phi)$ due to a warp as described by Eq. (4), we consider Jeans continuity equation of stellar dynamics. For the case of no radial motions we have

$$\frac{\partial \nu}{\partial t} + \frac{\partial(\nu \overline{v}_z)}{\partial z} + \frac{1}{r}\frac{\partial(\nu \overline{v}_\phi)}{\partial \phi} = 0. \tag{10}$$

If the stellar density ν is purely a function of $z' = z - Z_{\mathrm{w}}$ and $\partial \overline{v}_z / \partial z = 0$, the systematic vertical motion can be shown to be

$$\overline{v}_z(r, \phi) = \left(\frac{\overline{v}_\phi}{r} + \omega_{\mathrm{p}}\right) h(r) \cos\phi\,; \tag{11}$$

The systematic motion induced by a warp is simply the result of the stars rotating with respect to the warp structure. In our synthetic catalogues this systematic velocity is added to stars if they are in the warp (i.e. $r > r_{\mathrm{w}}$).

Fig. 11 shows the systematic $\langle W \rangle$ for a typical synthetic catalogue generated with a non-precessing warp having the parameters obtained from the sloped stellar distribution. This demonstrates that a non-precessing warp, consistent with the sloped distribution of our sample, should be easily detectable. The $\langle W \rangle$ of the synthetic catalogue lies systematically below the theoretical curve primarily due to a bias introduced by the error in the photometric distances.

7. Effect of bias, amplitude, and precession

The bias introduced by distance errors can be understood after some consideration. Stars whose distance is overestimated are likely to have larger distance errors than those whose distance are underestimated, as the distance error is normal in the distance modulus. Together with the fact that in a magnitude limited catalogue there are more stars closer to the Sun than further away, the skew in the distance errors means that stars with larger observed distances, d_{o}, are more likely to be stars whose true distance, d, is smaller. The effect of the misplacement of a star to larger distances is that its measured relative vertical motion $W_{\mathrm{o}}(d_{\mathrm{o}})$ will be smaller than its true relative vertical motion, $W(d)$. This can be seen from Eq. (8), for if differential Galactic rotation and vertical peculiar motions are neglected, we can write $W(d) = (4.74\mu_b / \cos b)d + W_\odot$, and similarly for $W_{\mathrm{o}}(d_{\mathrm{o}})$. Eliminating the common factor $(4.74\mu_b / \cos b)$ it can be shown that $W_{\mathrm{o}}(d_{\mathrm{o}}) - W(d) = (W(d) - W_\odot)(d_{\mathrm{o}}/d - 1)$. Hence, as long as $W(d) < W_\odot$ and $d_{\mathrm{o}}/d > 1$, $W_{\mathrm{o}}(d_{\mathrm{o}})$ will be less than $W(d)$. As we look out from the Galactic center r is proportional to d, so if $d_{\mathrm{o}} > d$ due to error, $r_{\mathrm{o}} > r$, and from

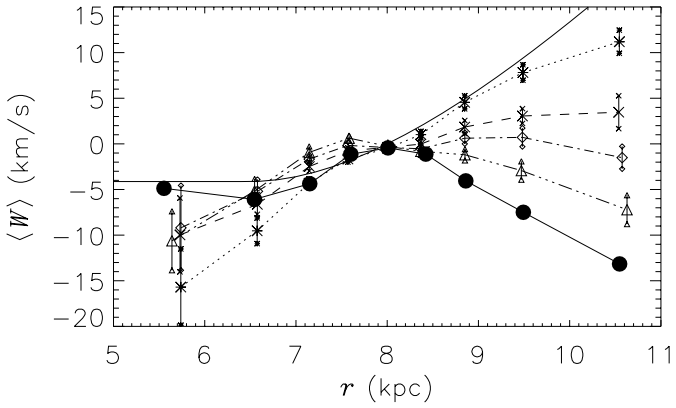

Fig. 12. The expected systematic vertical velocity from simulations for four cases: a standard warp ($*$), a warp with half amplitude ($\times$), a warp with half amplitude and a precession of $-13\,\mathrm{km\,s^{-1}\,kpc^{-1}}$ ($\diamond$), and a warp with half amplitude and a precession of $-25\,\mathrm{km\,s^{-1}\,kpc^{-1}}$($\triangle$). In the first 3 cases the σ_M is as given by Eq. (1), while in the fourth model an additional 0.5 magnitude error is added. Thirty simulated catalogues were generated for each case, and for each catalogue median velocities were determined for each radial bin. The systematic velocity of each bin shown above represents the mean of the 30 median velocities, while the error bars are the standard deviation of the 30 median velocities. The filled circles for the data and the solid line are the same as in Fig. 11, and are shown for comparison.

the above $W_\mathrm{o}(r_\mathrm{o}) < W(r)$. Finally, the kinematic signature of a warp increases outward, that is $W(r) < W(r_\mathrm{o})$, allowing us to write $W_\mathrm{o}(r_\mathrm{o}) < W(r_\mathrm{o})$; the average relative systematic velocity measured at a given r_o is smaller than it's true systematic relative velocity at r_o.

In addition to the above bias there are two other possible reasons why the observed systematic motions may be lower than that predicted for a long-lived warp. The first, trivially, is that the actual amplitude of the warp may be smaller than we have estimated from the observed slope of the spatial distribution. This may indeed be the case as radio data yield a warp amplitude between 0.3 and 0.4 kpc at a galactic radius of 10 kpc (Burton & Hartmann 1994), while our warp parameters produce an amplitude of.8 kpc. In Fig. 12 the signature expected from our standard warp ($r_\mathrm{h} = 15\,\mathrm{kpc}$) is shown together with the signature of a warp with half amplitude ($r_\mathrm{h} = 30\,\mathrm{kpc}$).

Lastly, the warp may be precessing in the direction of Galactic rotation. Fig. 12 shows the expected signal of a warp of half amplitude precessing at $-13\,\mathrm{km\,s^{-1}\,kpc^{-1}}$. While these three effects, taken together, have significantly reduced the expected velocity signature, we still have not recovered the negative velocities seen in our Hipparcos sample. Could higher precession rates, or higher errors in the photometric distances produce the velocity signature that we detect? The fourth model in Fig. 12 shows the effect of a precession rate of $-25\,\mathrm{km\,s^{-1}\,kpc^{-1}}$ on a warp of half amplitude with elevated photometric error ($\sigma_M = 1. + \max(0, (m - 6.5)/6) - M/12$). In this extreme case negative vertical motions are finally achieved.

8. Discussion

We have confirmed with a larger and more complete sample of distant OB stars that the observed kinematics and structure perpendicular to the Galactic plane are together inconsistent with the hypothesis of a long-lived non-precessing warp. However, with a revised model for the errors, negative systematic velocities can be produced, but only with excessively large precession rates, a smaller warp and large photometric errors. A precession rate even as high as $-20\,\mathrm{km\,s^{-1}\,kpc^{-1}}$ is questionable on physical grounds, for it would require that the warp was precessing faster than Galactic rotation at a galactocentric radius of only 11 kpc!

Could the photometric error parameter even be as high as one magnitude? The π_P–π_t distribution of models generated with such errors (see Fig. 7), compared to the observed π_P–π_t distribution (Fig. 5) would suggest not.

If we do not accept such large photometric errors and precession rates we are left with the same conclusions that we arrived at in our previous work; either the Galactic warp is not long-lived, or there are other systematic motions present in the Galactic disk. Galactic companions could be responsible for a short-lived warp, or at least modify the velocities, but the regularity of the Galactic warp out to at least 16 kpc from the Galactic center makes this seem unlikely. Nevertheless, numerical simulations will have to be carried out to explore this possibility.

Alternatively, the presence of other systematic vertical oscillations in the Galactic disk could mask the kinematic signature of the warp, but should also be evidenced by accompanying deviations from the Galactic plane. The warp amplitudes as inferred from the OB stars found here (0.4 to 0.8 kpc at $r = 10\,\mathrm{kpc}$) are larger than those found in the HII gas (0.3 to 0.4 kpc at $r = 10\,\mathrm{kpc}$, Burton & Hartmann 1994) and the dust (0.3 kpc at $r = 10\,\mathrm{kpc}$, Freudenreich 1998), and may suggest the presence of such structures. In addition Dehnen (1998) also finds that the kinematics of nearby stars are not consistent with a Galactic warp that begins within the Solar Circle needed to produce a local tilt in the stellar distribution. Indeed, the observed slopes and anomalous kinematic signature may not be due to a warp at all, but to some other as yet unidentified phenomenon.

The possibility of other systematic motions being present in the disk complicates any evaluation of the kinematics of the Galactic warp. Until a deeper and more accurate astrometric survey is completed the possibility of other kinematic effects cannot be excluded nor, if present, be disentangled from the expected kinematic signature of the warp in the stellar distribution. Such a survey will eventually be given by a future astrometric mission like GAIA, which will also, via parallaxes, largely dispense with the bias introduced by the photometric distance errors.

Acknowledgements. Thanks are extended to James Binney and Stefano Casertano for useful discussions, and the reviewer who contributed to the quality of this contribution. R. Drimmel and R. L. Smart acknowledge support from the University of Turin. R. L. Smart also acknowledges support from the British Royal Society.

References

Binney J., 1992, ARA&A 30, 51
Blaauw A., 1993, In: Cassinelli J.P., Churchwell E.B. (eds.) ASP Conf. Ser. 35: Massive Stars, Their Lives in the Interstellar Medium
Burton W.B., Hartmann D., 1994, Ap&SS 217, 189
Dehnen W., 1998, AJ 115, 2384
Dehnen W., Binney J.J., 1998, MNRAS 298, 387
Djorgovski S., Sosin C., 1989, ApJ 341, L13
Drimmel R., Smart R.L., Lattanzi M.G., 1997, In: Perryman M.A.C.(ed.) Hipparcos Venice '97, ESA SP-402, p. 607
Drimmel R., Smart R.L., Lattanzi M.G., 1999, In: Dvorak R. (ed.) Modern Astrometry and Astrodynamics. Kluwer
ESA, 1997, The Hipparcos Catalogue. ESA SP-1200
Freudenreich H., 1998, ApJ 492, 495
Freudenreich H., Berriman G., Dwek E., et al., 1994, AJ 429, L69
Houk N., Smith-Moore M., 1988, Michigan Spectral Survey. Vol. 4, University of Michigan, Department of Astronomy, Ann Arbor
Lang K.R., 1992, Astrophysical Data I, Planets and Stars. Springer-Verlag, Berlin-Heidelberg-New York
Mignard F., 1997, In: Perryman M.A.C. (ed.) Hipparcos Venice '97, ESA SP-402, p. 5
Schmidt-Kaler T., 1982, In: Landolt-Bornstein: Numerical Data and Functional Relationships in Science and Technology
Smart R.L., Lattanzi M.G., 1996, A&A 314, 104
Smart R.L., Drimmel R., Lattanzi M.G., 1997, In: Perryman M.A.C. (ed.) Hipparcos Venice '97, ESA SP-402, p. 715
Smart R.L., Drimmel R., Lattanzi M.G., Binney J.J., 1998, Nat 392, 471
Smart R.L., Drimmel R., Lattanzi M.G., 1999, In: Dvorak R. (ed.) Modern Astrometry and Astrodynamics. Kluwer
Smith H., 1985, A&A 152, 413
Spergel D.N., Malhotra R., Blitz L., 1997, In: Minnitti D., Rix H. (eds.) Spiral Galaxies in the Near-IR. ESO-Garching
Torra J., Gomez A.E., Figueras F., et al., 1997, In: Perryman M.A.C. (ed.) Hipparcos Venice '97, ESA SP-402, p. 513
Wouterloot J.G.A., Brand J., Burton W.B., Kwee K.K., 1990, A&A 230, 21